Chinese Chemical Letters 33 (2022) 2060–2064

Contents lists available at ScienceDirect

Chinese Chemical Letters

journal homepage: www.elsevier.com/locate/cclet

Boosting the photoelectrochemical water oxidation performance of bismuth vanadate by $ZnCo_2O_4$ nanoparticles

Jingwei Huang[a,b], Yani Wang[a,b], Kaiyi Chen[a], Tingting Liu[b], Qizhao Wang[a,b,c,*]

[a] School of Environment Science and Engineering, Chang'an University, Xi'an 710064, China
[b] College of Chemistry and Chemical Engineering, Northwest Normal University, Lanzhou 730070, China
[c] Tianjin Key Laboratory of Building Green Functional Materials, Tianjin Chengjian University, Tianjin 300384, China

ARTICLE INFO

Article history:
Received 8 June 2021
Revised 21 July 2021
Accepted 17 August 2021
Available online 21 August 2021

Keywords:
Photoelectrochemical water oxidation
$BiVO_4$
$ZnCo_2O_4$
p-n junction

ABSTRACT

Due to the involvement of four-electron transfer process at photoanode, water oxidation is the rate-limiting step in water splitting reaction. To settle this dilemma, $ZnCo_2O_4$ nanoparticles are combined with $BiVO_4$ to form a p-n $ZnCo_2O_4/BiVO_4$ heterojunction photoanode, which is proved by an input voltage−output current test. The built-in electric field formed within the heterojunction structure promotes the effective separation of electrons and holes. $ZnCo_2O_4$ is also an effective water oxidation cocatalyst, since it could cause the holes entering the electrode/electrolyte interface rapidly for the subsequent water oxidation reaction. The photocurrent density of $ZnCo_2O_4/BiVO_4$ composite photoanode reaches 3.0 mA/cm^2 at 1.23 V *vs.* RHE in 0.5 mol/L sodium sulfate under AM 1.5G simulated sunlight, about 2.1 times greater than that of $BiVO_4$ (1.4 mA/cm^2). These results suggest the potential of $ZnCo_2O_4$ nanoparticles for improving photoelectrochemical water splitting anode materials.

The conversion of solar energy into hydrogen by photoelectrochemical (PEC) water splitting is a promising way to produce hydrogen, which can simultaneously solve the current energy shortage and environmental problems caused by fossil fuel combustion [1–3]. In the process of PEC water splitting, water oxidation (producing oxygen) and water reduction (producing hydrogen) reaction are involved. The water oxidation reaction involves a kinetic unfavorable four-electron transfer process, which determines the entire water splitting reaction rate [4,5]. Researches are mainly focused on photoanodes where water oxidation reaction takes place. Metal oxides such as TiO_2 [6,7], Fe_2O_3 [8,9], WO_3 [10], ZnO [11] and $BiVO_4$ [12-14] are often used as photoanode materials for PEC water oxidation. Among them, $BiVO_4$ is a very excellent photoanode material with beneficial energy band structure and a band gap of 2.4 eV, enabling it to absorb part of visible light [15-17]. However, the slow migration rate of photogenerated electrons and holes in $BiVO_4$ and sluggish kinetics for water oxidation render $BiVO_4$ far below its theoretical photocurrent density [18,19]. Strategies such as controlling morphology [20], constructing heterostructures [10] have been used to improve the performance of $BiVO_4$. Besides, loading cocatalyst is an effective way to improve the surface reaction kinetics of $BiVO_4$ for PEC water splitting [21,22].

Cobalt-based cocatalysts, such as cobalt oxides [23–25], cobalt hydroxides [26,27], cobalt phosphide [28,29], Co-Pi [30,31], Co-based double hydroxide (LDH) [32], have been intensively studied as water oxidation catalysts due to their outstanding catalytic performance. Specially, ternary spinel MCo_2O_4 (M = Ni, Mn, Zn, *etc.*) have improved bearing conductivity and possessing more active sites than Co_3O_4, resulting in a better water oxidation capability [33–35]. Among them, $ZnCo_2O_4$ has a definite structure in which Zn^{2+} only replaces Co^{2+} in the tetrahedral sites in Co_3O_4, rarely affecting the Co^{3+} active site in the octahedral sites in Co_3O_4 [36]. Therefore, as compared to Co_3O_4, the use of $ZnCo_2O_4$ could reduce the use of rare and relative expensive Co element without the compromise of catalytic activity.

In addition to loading cocatalyst, enhancing built-in electric field of a photoanode by constructing a heterojunction structure is also usually adopted. WO_3@$BiVO_4$ heterojunction photoanode [37], $Fe_2O_3/BiVO_4$ heterojunction photoanode [38], g-C_3N_4@$BiVO_4$ heterojunction photoanode [39] *etc.* are recently reported to be favorable for the separation of photo-generated carriers due to the formation of built-in electric field between these different semiconductors in heterojunction. However, the water oxidation reaction on surface of these photoanodes is still sluggish. To address this problem, cocatalysts are still needed. For example, NiFe-

* Corresponding author at: School of Environment Science and Engineering, Chang'an University, Xi'an 710064, China
E-mail address: qzwang@chd.edu.cn (Q. Wang).

https://doi.org/10.1016/j.cclet.2021.08.082
1001-8417/

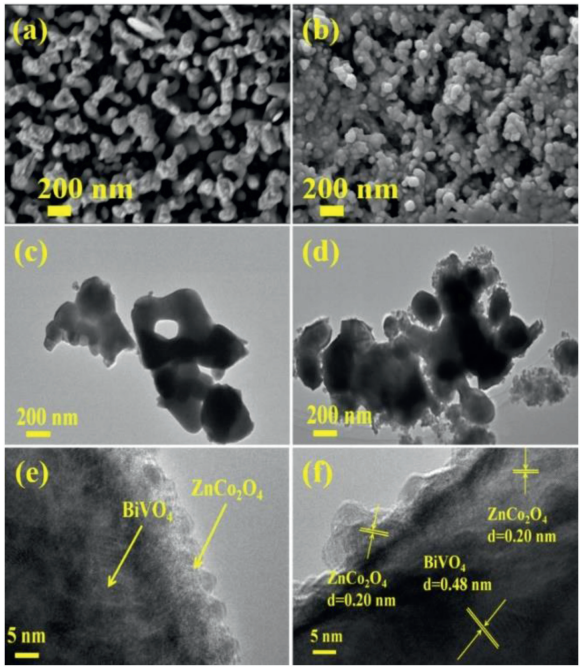

Fig. 1. SEM images of (a) $BiVO_4$, (b) $ZnCo_2O_4/BiVO_4$-35. TEM images of (c) $BiVO_4$, (d) $ZnCo_2O_4/BiVO_4$-35. (e, f) HR-TEM images of $ZnCo_2O_4/BiVO_4$-35.

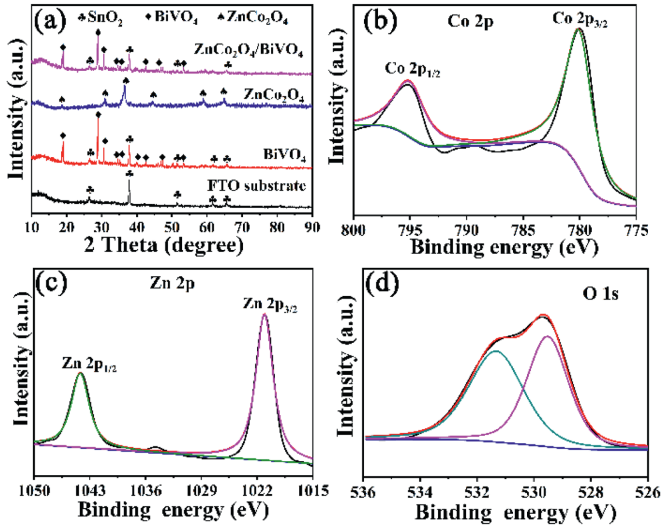

Fig. 2. (a) XRD patterns of FTO substrate, $BiVO_4$, $ZnCo_2O_4$ and $ZnCo_2O_4/BiVO_4$ composites and XPS spectra of (b) Co 2p, (c) Zn 2p, (d) O 1s in $ZnCo_2O_4/BiVO_4$.

LDH was used to load on $Fe_2O_3/BiVO_4$ heterojunction photoanode [40]. $WO_3/BiVO_4$ was modified by FeOOH to construct ternary $WO_3/BiVO_4$/FeOOH hierarchical photoanode [41]. Considering the complicated fabrication process of above mentioned photoanodes, loading a semiconductor cocatalyst that could enhance the built-in electric field as well as act as cocatalyst is a new guiding ideology to construct a high performance photoanode for water oxidation.

In this work, $ZnCo_2O_4$ nanoparticles, acting as a p-type semiconductor and a cocatalyst simultaneously, were loaded on $BiVO_4$ to form $ZnCo_2O_4/BiVO_4$ composite photoanode by electrophoretic deposition. The formation of p-n junctions between $ZnCo_2O_4$ and $BiVO_4$ is systematically confirmed, which introduces built-in electric field that is beneficial to the separation of photogenerated carriers. This composite photoanode shows high photocurrent for PEC water oxidation due to the improvement in charge separation efficiency and surface reaction efficiency.

As can be seen from Fig. 1a, $BiVO_4$ presents a coral-like structure composed of porous nanoparticles. The nanoparticles are interconnected on the surface of the FTO to form pores and channels. These abundant channels facilitate the contact between the semiconductor and electrolyte. From Fig. 1b, it can be clearly seen that $ZnCo_2O_4$ nanoparticles are uniformly loaded onto the surface of $BiVO_4$ film by the electrophoretic deposition method. TEM image (Fig. 1c) shows that $BiVO_4$ has a pore structure and smooth surface. However, a thin layer of nanoparticles appears on the surface of $BiVO_4$ after loading $ZnCo_2O_4$ as shown in Fig. 1d. Figs. 1e and f show the HR-TEM images of $ZnCo_2O_4/BiVO_4$ photoanode. The spacing of 0.20 nm and 0.48 nm correspond to the (400) plane of $ZnCo_2O_4$ (PDF card No. 23-1390) and the (110) plane of $BiVO_4$ (PDF No. 14-0688), respectively, demonstrating the successful combination of $ZnCo_2O_4$ nanoparticles and $BiVO_4$ film to form $ZnCo_2O_4/BiVO_4$ photoanode.

In order to clearly grasp the crystal structure of the sample, we performed XRD testing on the photoanode material. As shown in Fig. 2a, FTO substrate has the diffraction peaks located at 26.6°, 37.8°, 51.8°, 61.7° and 65.7° corresponding to the (110), (200), (211), (310) and (301) lattice diffractions of SnO_2 (JCPDS No. 46–1088), respectively. $BiVO_4$ shows diffraction peaks located at 18.7°, 28.8°, 30.5°, 34.5°, 35.2°, 40.0°, 42.5°, 46.0°, 47.3°, 50.3°, 53.3°, 58.3° and 59.3°, indicating the formation of monoclinic phase $BiVO_4$ (JCPDS: 14-0688). The synthesized $ZnCo_2O_4$ powders have diffraction peaks mainly located at 19.0°, 31.2°, 36.8°, 44.7°, 59.3° and 65.1°. These diffraction peak positions correspond to the (111), (220), (311), (400), (511) and (440) crystal planes of the $ZnCo_2O_4$ (JCPDS: 23-1390), proving that the $ZnCo_2O_4$ nanoparticles were successfully synthesized. The XRD pattern of $ZnCo_2O_4/BiVO_4$ composite electrode does not show obvious characteristic diffraction peaks of $ZnCo_2O_4$ due to small loading amount of $ZnCo_2O_4$ nanoparticles on $BiVO_4$. X-ray photoelectron spectroscopy (XPS) test was used to determine the elements status of $ZnCo_2O_4/BiVO_4$ electrode. It can be seen from Fig. 2b that two peaks of Co 2p in $ZnCo_2O_4$ are located 795.0 and 780.0 eV, respectively belonging to the Co $2p_{1/2}$ and Co $2p_{3/2}$ peaks of Co^{3+} in the octahedral site, and proving that the cobalt in the compound is +3 valence [36]. The binding energies of the Zn $2p_{3/2}$ and Zn $2p_{1/2}$ peaks in the compounds are located at 1021.1 eV and 1044.2 eV, indicating that Zn in the $ZnCo_2O_4$ is +2 valence in the compound (Fig. 2c) [42]. The O 1s spectrum in the $ZnCo_2O_4/BiVO_4$ photoanode can be fitted into two diffraction peaks (Fig. 2d). The peak at 531.4 eV in the spectrum is derived from adsorbed OH^- on the electrode, while the peak at 529.7 eV is assigned to oxide lattice [43].

The light absorption range of $ZnCo_2O_4/BiVO_4$ photoanode is broadened slightly by supporting $ZnCo_2O_4$ cocatalyst (Fig. S1a in Supporting information). The light absorption intensity of the composite is also higher than that of $BiVO_4$, indicating that $ZnCo_2O_4$ improves the light absorption capacity of $BiVO_4$. The band gap of $BiVO_4$ is about 2.46 eV, whilst $ZnCo_2O_4/BiVO_4$ electrode shows an apparent band gap of 2.43 eV, demonstrating $ZnCo_2O_4$ can improve the light utilization efficiency of $BiVO_4$ photoanode (Fig. S1b in Supporting information). In order to investigate whether the catalytic active area of $BiVO_4$ film would be changed after loading $ZnCo_2O_4$, cyclic voltammetry (CV) tests of $BiVO_4$ and $ZnCo_2O_4/BiVO_4$ electrodes were carried out at different scan rates as shown in Figs. S1c and e (Supporting information). The catalytic active area of $BiVO_4$ and $ZnCo_2O_4/BiVO_4$ electrodes can be estimated from double layer capacitances that are linearly related to the slopes of difference values between anode current (J_a) and cathode current (J_c) in CVs against the scan rate as shown in Figs. S1d and f (Supporting information). Taking the current difference as y-axis and scanning rate as x-axis, the linear slope is twice over

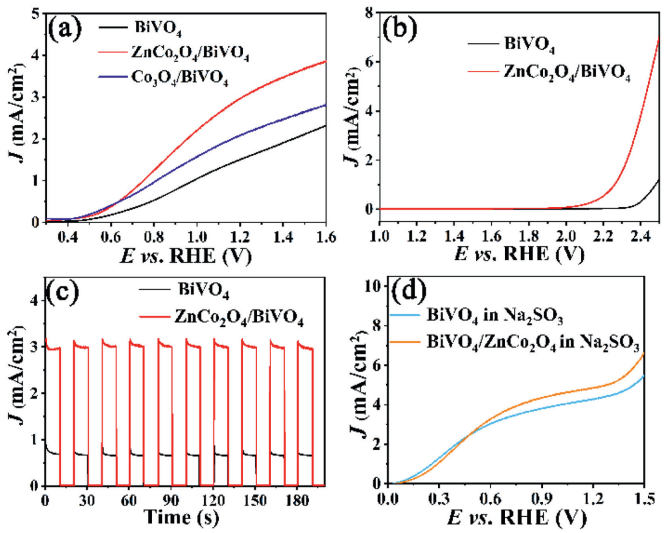

Fig. 3. LSV curves of $BiVO_4$, $ZnCo_2O_4/BiVO_4$ photoelectrodes (a) with and (b) without light irradiation; (c) Chopped *I-t* curves of $BiVO_4$, $ZnCo_2O_4/BiVO_4$ photoelectrodes at 1.23 V *vs.* RHE in 0.5 mol/L Na_2SO_4. (d) LSV curves of photoanodes for sulfite oxidation (with 1 mol/L Na_2SO_3).

the double layer capacitances [44]. It can be seen from Figs. S1d and f that the slope of $ZnCo_2O_4/BiVO_4$ is larger than that of $BiVO_4$, demonstrating the catalytic active area of $BiVO_4$ photoanode increases after loading $ZnCo_2O_4$.

The LSV curves of $BiVO_4$ and $ZnCo_2O_4/BiVO_4$ photoanodes were tested under AM 1.5G simulated sunlight (100 mW/cm^2) from back side of the sample. As shown in Fig. 3a, the photocurrent density of $BiVO_4$ is 1.4 mA/cm^2 at 1.23 V *vs.* RHE, while the photocurrent density of 3.0 mA/cm^2 is obtained for the $ZnCo_2O_4/BiVO_4$ photoanode. Besides, the onset potential of $BiVO_4$ photoanode shifts *ca.* 0.1 V after loading $ZnCo_2O_4$. $Co_3O_4/BiVO_4$ photoanode was also fabricated for comparison using the same electrophoretic deposition method as shown in Fig. 3a, giving a photocurrent of 2.2 mA/cm^2 at 1.23 V *vs.* RHE at same reaction condition. Obviously, $ZnCo_2O_4$ shows more higher catalytic activity than that of Co_3O_4. The photocurrent density of $ZnCo_2O_4/BiVO_4$ is 2.1 times that of $BiVO_4$. This indicates that the performance of $BiVO_4$ for PEC water splitting can be enhanced by $ZnCo_2O_4$. The comparison of $ZnCo_2O_4/BiVO_4$ photoanode with other $BiVO_4$ and Co based photoanodes is shown in Table S1 (Supporting information). In order to investigate the effect of deposition time on the catalytic performance of $ZnCo_2O_4/BiVO_4$, the electrophoretic deposition time of $ZnCo_2O_4$ was set be to 15, 20, 25, 30, 35 and 40 s for comparison. These composite photoanodes are named as $ZnCo_2O_4/BiVO_4$-15, $ZnCo_2O_4/BiVO_4$-20, $ZnCo_2O_4/BiVO_4$-25, $ZnCo_2O_4/BiVO_4$-30, $ZnCo_2O_4/BiVO_4$-35 and $ZnCo_2O_4/BiVO_4$-40 accordingly. As demonstrated in Fig. S2 (Supporting information), the photocurrent density of $ZnCo_2O_4/BiVO_4$-35 has the highest photocurrent at 1.23 V *vs.* RHE, indicating that $ZnCo_2O_4/BiVO_4$-35 has the best PEC water splitting performance. When the deposition time is less than 35 s, small photocurrents were obtained probably due the lower content of $ZnCo_2O_4$. However, when the amount of the supported $ZnCo_2O_4$ is excessive, the transport of holes to the electrode surface is hindered, leading to low photocurrents. $ZnCo_2O_4/BiVO_4$-35 was used in all the experiments without further description. Fig. 3b is LSV curves of the electrodes in the absence of light. The initial potential of $BiVO_4$ is about 2.4 V, while the initial potential of the $ZnCo_2O_4/BiVO_4$ composite photoanode is about 2.1 V. The initial potential of $ZnCo_2O_4/BiVO_4$ negatively shifts 300 mV compared to that of $BiVO_4$. This indicates that $ZnCo_2O_4$ can reduce the overpotential of PEC water splitting. The chopped *I-t* curves of the photoanodes were tested at 1.23 V *vs.* RHE. It can be clearly seen from the *I-t* curves in Fig. 3c that the photocurrent density of the composite $ZnCo_2O_4/BiVO_4$ photoanode is stable and higher than that of $BiVO_4$ at constant voltage. Fig. 3d shows the LSV curves of $BiVO_4$ and $ZnCo_2O_4/BiVO_4$ photoanodes tested in 0.5 mol/L Na_2SO_4 solution with 1 mol/L Na_2SO_3. As a hole trapping agent, Na_2SO_3 is easily oxidized by holes. When Na_2SO_3 is present, the photogenerated holes reaching the surface of $BiVO_4$ and $ZnCo_2O_4/BiVO_4$ are all involved in the oxidation of Na_2SO_3. Therefore, the photocurrent density for Na_2SO_3 oxidation represents the amount of photogenerated holes reaching on the surface of $BiVO_4$ and $ZnCo_2O_4/BiVO_4$. In the presence of Na_2SO_3, the photocurrent density of $ZnCo_2O_4/BiVO_4$ is higher than that of $BiVO_4$, indicating that the amount of photogenerated holes reaching the surface of $ZnCo_2O_4/BiVO_4$ is higher than that of $BiVO_4$. This means that the $ZnCo_2O_4/BiVO_4$ heterojunction structure promotes the separation of photogenerated charges. Fig. S3 (Supporting information) shows the chopped LSV curves of $BiVO_4$ and $ZnCo_2O_4/BiVO_4$ with chopped light illumination. When the simulated sunlight was used to illuminate the photoanode, the photocurrent density of the $BiVO_4$ and $ZnCo_2O_4/BiVO_4$ electrodes immediately increased. When the light is blocked, the photocurrent density of the both photoanodes immediately reduced to almost 0 mA/cm^2, suggesting that the photoanodes is very sensitive to light. The photocurrent densities of the electrodes are disparate at different voltages. At the same potential, the photocurrent density of the $ZnCo_2O_4/BiVO_4$ photoanode is distinctly higher than that of the $BiVO_4$ electrode, implying $ZnCo_2O_4$ nanoparticles can significantly improve the PEC water oxidation performance of $BiVO_4$ photoanode.

The efficiency of PEC water splitting is determined by light capture efficiency, charge separation efficiency in the bulk (η_{bulk}) and surface reaction efficiency ($\eta_{surface}$) of photoelectrode. To analyze these efficiencies, the maximum theoretical photocurrents J_{abs} under AM 1.5G simulated sunlight was calculated from UV diffuse reflection data of $BiVO_4$ and $ZnCo_2O_4/BiVO_4$ photoanodes (Fig. S4 in Supporting information). η_{bulk} was calculated through dividing the photocurrent for Na_2SO_3 oxidation ($J_{Na_2SO_3}$, Data in Fig. 3d) by J_{abs} [44]. $\eta_{surface}$ represents the ratio of surface holes participated in the reaction, which is obtained through dividing photocurrent for water oxidation (data in Fig. 3a) by $J_{Na_2SO_3}$. Fig. 4a shows that η_{bulk} of $ZnCo_2O_4/BiVO_4$ reaches 70% at 1.23 V *vs.* RHE, while the η_{bulk} of pure $BiVO_4$ is 50%, indicating the loading of $ZnCo_2O_4$ can enhance charge separation efficiency of $BiVO_4$. Fig. 4b represents the $\eta_{surface}$ of the $ZnCo_2O_4/BiVO_4$ photoanode reaches 50% at 1.23 V *vs.* RHE, while the $\eta_{surface}$ of the $BiVO_4$ photoanode is merely 25%. As a water oxidation cocatalyst, $ZnCo_2O_4$ improves the kinetics of water splitting reaction. Based on LSV curve shown in Fig. 3a, applied bias photon-to-current efficiency (ABPE) values can be obtained [45]. In Fig. 4c, the maximum efficiency of the $BiVO_4$ film is 0.1% at 1.1 V *vs.* RHE, while the $ZnCo_2O_4/BiVO_4$ photoanode attains a maximum ABPE value of 0.6% at 0.9 V *vs.* RHE. The maximum efficiency of $ZnCo_2O_4/BiVO_4$ composite photoanode is 6 times that of $BiVO_4$. This indicates that $ZnCo_2O_4$ improves the photoelectrochemical performance of $BiVO_4$. The IPCE values of $BiVO_4$ and $ZnCo_2O_4/BiVO_4$ photoanodes were tested at 1.23 V *vs.* RHE. As can be seen from Fig. 4d, the IPCE value of $ZnCo_2O_4/BiVO_4$ electrode is higher than that of $BiVO_4$ in the wavelength range of 320~510 nm. The IPCE value of $ZnCo_2O_4/BiVO_4$ electrode can reach 40% at 380 nm. Absorbed photon-to-current conversion efficiency (APCE) of $BiVO_4$ and $ZnCo_2O_4/BiVO_4$ electrodes were calculated through dividing IPCE values by light absorption values and the resulting APCE values are given in Fig. S5 (Supporting information). Almost half absorbed photons can be converted to current by $ZnCo_2O_4/BiVO_4$ electrode, about 20% higher than that of $BiVO_4$, indicating that the light utilization rate of the electrode is improved

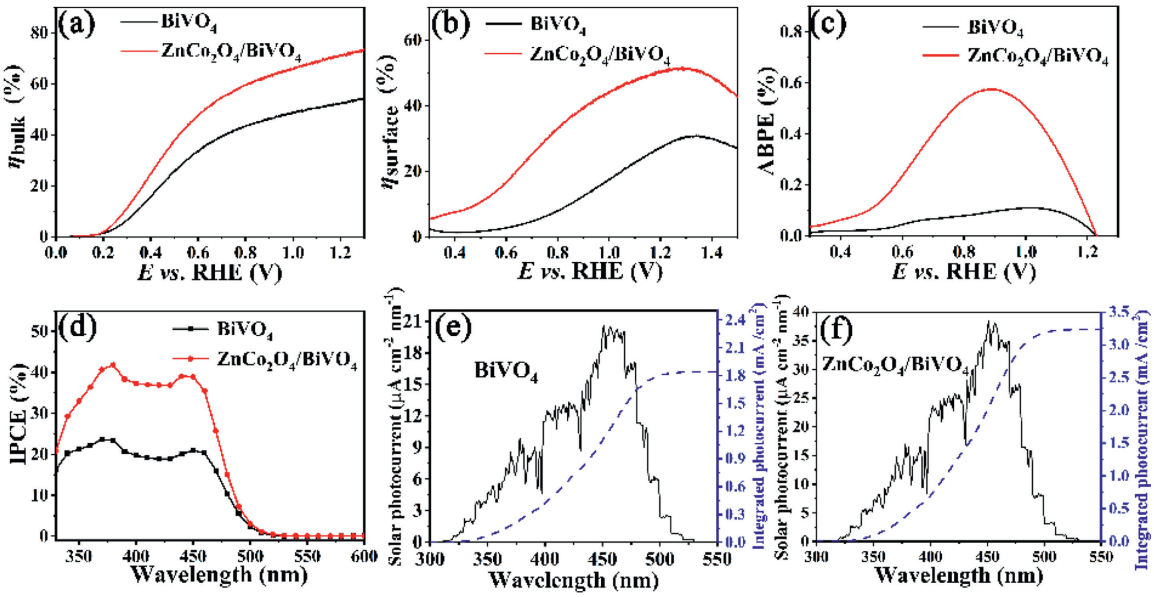

Fig. 4. (a) Charge separation efficiency in the bulk (η_{bulk}) and (b) surface reaction efficiency ($\eta_{surface}$) of $BiVO_4$ and $ZnCo_2O_4/BiVO_4$ photoanodes. (c) ABPE curves of pure $BiVO_4$ and $ZnCo_2O_4/BiVO_4$ photoelectrodes. (d) IPCE values of $BiVO_4$ and $ZnCo_2O_4/BiVO_4$ photoanodes; Solar photocurrents of (e)$BiVO_4$ and (f) $ZnCo_2O_4/BiVO_4$ anodes (left ordinate) and integrated photocurrent at 1.23 V *vs.* RHE (right ordinate).

after loading $ZnCo_2O_4$. To confirm the reliability of our tests, the integrations of IPCE of $BiVO_4$ and $ZnCo_2O_4/BiVO_4$ photoanodes with the AM 1.5G solar current were carried out. As shown in Figs. 4e and f, the photocurrents of $BiVO_4$ and $ZnCo_2O_4/BiVO_4$ photoanodes obtained by integrating AM 1.5G solar currents are 1.8 and 3.2 mA/cm^2, which are approximate equivalent to the photocurrents in LSV measurement, indicating the tests are reliable.

The relative magnitude of the charge transfer rate of $BiVO_4$ and $ZnCo_2O_4/BiVO_4$ photoanodes was investigated by electrochemical impedance spectroscopy (EIS). The Nyquist plots of EIS spectra of $BiVO_4$ and $ZnCo_2O_4/BiVO_4$ photoanodes are a semi-circular arc whatever in dark conditions or under AM 1.5G simulated sunlight (Figs. S6a and b in Supporting information). The impedance of the circuit can be explained by the simplified Randles circuit model, in which R_Ω represents the solution resistance. R_{ct} represents charge-transfer resistance at the interface of semiconductor and electrolyte and C_{ct} represents the capacitance of the bulk $BiVO_4$ [46]. The smaller the diameter of the arc, the stronger the charge transfer capability is. $ZnCo_2O_4/BiVO_4$ exhibits a smaller arc diameter than $BiVO_4$, indicating that the charge transfer rate in the photoanode increases after the $ZnCo_2O_4$ cocatalyst is supported. It is worth noting that the arc diameter is smaller under light irradiation, indicating charge transfer become easy with light irradiation. The PEC water splitting reaction of $ZnCo_2O_4/BiVO_4$ photoanode was carried out in a closed reactor. Prior to the water splitting reaction, the reactor was purged with N_2 for 1 hour to remove air from the reactor. The PEC water splitting reaction was carried out for 3 h at 1.23 V *vs.* RHE. 1 mL of gas was withdrawn from the reactor every half hour, and the gas was quickly pumped into the gas chromatograph to detect the amount of hydrogen and oxygen produced. After 3 h of reaction, 153.7 μmol of H_2 and 79.8 μmol of O_2 were produced with the mole ratio of H_2 to O_2 of 1.9:1 (Fig. S6c in Supporting information). The average Faradaic efficiency of PEC cell for H_2 and O_2 production (Fig. S6d in Supporting information) is about 90% and 86%, respectively, which indicates that the photoanode $ZnCo_2O_4/BiVO_4$ has good water splitting efficiency.

Mott-Schottky tests were performed to study the semiconductor type of $ZnCo_2O_4$, $BiVO_4$ and $ZnCo_2O_4/BiVO_4$ photoanodes. As demonstrated in Fig. 5a, $ZnCo_2O_4$ shows a negative slope, indicating that $ZnCo_2O_4$ is p-type semiconductor. While $BiVO_4$ photoanode shows positive slope, meaning the n-type property of $BiVO_4$ (Fig. 5b). The intersection of Mott-Schottky curves and x-axis are close to 0.38 V *vs.* RHE with/without loading $ZnCo_2O_4$, demonstrating the flat band potentials (V_{fb}) of $BiVO_4$ photoanodes are 0.38V.

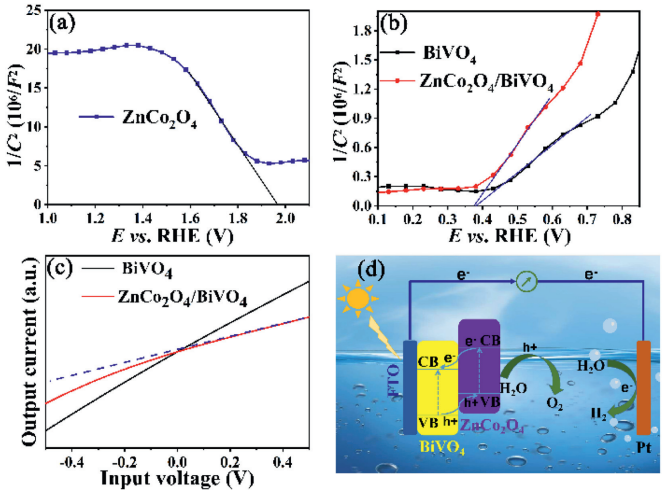

Fig. 5. Mott-Schottky plots of (a) $ZnCo_2O_4$ and (b) $BiVO_4$, $ZnCo_2O_4/BiVO_4$; (c) Input voltage–output current characteristic curves of $BiVO_4$ and $ZnCo_2O_4/BiVO_4$ anodes. The dotted line is used as a linear reference; (d) Heterojunction illustration and water splitting mechanism of $ZnCo_2O_4/BiVO_4$ photoanode.

The V_{fb} value of $BiVO_4$ is 0.38V. Considering that the V_{fb} of n-type semiconductor is slightly positive (~0.1–0.3 V) than the CB potential, the conduction band (CB) potential of $BiVO_4$ is about 0.18 V [47]. The band gap of $BiVO_4$ is 2.46 eV (Fig. S1b). According to the relationship between CB and valence band (VB), the VB of $BiVO_4$ can be calculated to be 2.64 V. The p-type semiconductor $ZnCo_2O_4$ has a V_{fb} value of 1.98 V (Fig. 5a). Because VB position of a p-type semiconductor is approximately 0.2 V higher than its V_{fb} value, the VB position of $ZnCo_2O_4$ is 2.18 V. $ZnCo_2O_4$ has a band gap width of 2.10 eV, so the CB position of $ZnCo_2O_4$ is calculated

to be 0.08 V. The staggered energy levels of $BiVO_4$ and $ZnCo_2O_4$ allows them to form p-n junction.

The formation of p-n junctions between $BiVO_4$ and $ZnCo_2O_4$ was proved by input voltage-output current test as shown in Fig. 5c. $BiVO_4$ photoanode shows a linear relationship between input voltage and output current due to the ohmic contact between $BiVO_4$ and FTO substrate [48]. On the contrary, $ZnCo_2O_4/BiVO_4$ anode represents a nonlinear relation between output current and input voltage, indicating the interface contact type between $ZnCo_2O_4$ and $BiVO_4$ is p-n junction [49]. Built-in electric field in the p-n junction favors the transfer of holes from $BiVO_4$ to $ZnCo_2O_4$ for water oxidation.

The PEC water splitting mechanism of $ZnCo_2O_4/BiVO_4$ is proposed as shown in Fig. 5d. $BiVO_4$ and $ZnCo_2O_4$ are excited to generate electrons and holes by illuminating from the back of the photoanode. The electrons in conduction band of $ZnCo_2O_4$ migrate to the conduction band of $BiVO_4$, and then transfer to the counter electrode under external circuit for H_2 evolution reaction. The holes in valence band of $BiVO_4$ transfer to the valence band position of $ZnCo_2O_4$ with the assistance of built-in electric field for water oxidation reaction (O_2 evolution reaction). After a long-time reaction, the photocurrent of $ZnCo_2O_4/BiVO_4$ anode presents only a small decrease (Fig. S7 in Supporting information).

In summary, we have constructed a p-n heterojunction $ZnCo_2O_4/BiVO_4$ photoanode by a simple electrophoretic deposition method. The formation of p-n junction between $BiVO_4$ and $ZnCo_2O_4$ is proved by input voltage−output current test. Compared with $BiVO_4$, this composite photoanode $ZnCo_2O_4/BiVO_4$ has better photoelectrochemical water splitting performance. The photocurrent density of $ZnCo_2O_4/BiVO_4$ reaches 3.0 mA/cm^2 at 1.23 V *vs.* RHE, about 2.1 times greater than that of $BiVO_4$. The formation of a p-n heterojunction between the $BiVO_4$ and $ZnCo_2O_4$ improves the separation efficiency of carriers while the cocatalyst $ZnCo_2O_4$ accelerates the surface reaction kinetics, leading to enhanced charge separation efficiency and surface reaction efficiency. After 3 h reaction, the produced H_2 and O_2 achieve 153.7 and 79.8 μmol, respectively. All results demonstrate that $ZnCo_2O_4$ can boost the photoelectrochemical water oxidation performance of $BiVO_4$.

Declaration of competing interest

The authors declare that they have no known competing financial interests or personal relationships that could have appeared to influence the work reported in this paper.

Acknowledgments

This work was financially supported by the National Natural Science Foundation of China (Nos. 21808189 and 21663027), Natural Science Basic Research Fund of Shaanxi Province (No. 2020JZ20), and Fundamental Research Funds for the Central Universities of Chang'an University (No. 300102299304).

Supplementary materials

Supplementary material associated with this article can be found, in the online version, at doi:10.1016/j.cclet.2021.08.082.

References

[1] F. Niu, D. Wang, F. Li, et al., Adv. Energy Mater. 10 (2020) 1900399.
[2] S. Singh, H. Chen, S. Shahrokhi, et al., ACS Energy Lett 5 (2020) 1487–1497.
[3] Z. Wang, L. Wang, Sci. China Mater. 61 (2018) 806-821.
[4] H. Kaneko, T. Minegishi, K. Domen, Chem. Eur. J. 24 (2018) 5697–5706.
[5] Z. Jiang, Q. Chen, Q. Zheng, et al., Acta Phys. Chim. Sin. 37 (2021) 2010059.
[6] Y. Li, R. Zhang, J. Li, et al., Chinese Chem. Lett. 32 (2021) 1165–1168.
[7] N. Zheng, X. He, W. Guo, Z. Hu, Chinese Chem. Lett. 32 (2021) 1993–1997.
[8] K. Sivula, R. Zboril, F.Le Formal, et al., J. Am. Chem. Soc. 132 (2010) 7436–7444.
[9] Z. Luo, T. Wang, J. Zhang, et al., Angew. Chem. Int. Ed. 56 (2017) 12878–12882.
[10] J. Huang, P. Yue, L. Wang, H. She, Q. Wang, Chin. J. Catal. 40 (2019) 1408–1420.
[11] J. Long, W. Wang, S. Fu, L. Liu, J. Colloid Interf. Sci. 536 (2019) 408–413.
[12] J. Huang, T. Liu, R. Wang, et al., J. Colloid Interf. Sci. 570 (2020) 89–98.
[13] H. She, M. Jiang, P. Yue, et al., J. Colloid Interf. Sci. 549 (2019) 80–88.
[14] L. Wang, X. Shi, Y. Jia, et al., Chinese Chem. Lett. 32 (2021) 1869–1878.
[15] B. Lamm, B.J. Trzesniewski, H. Doscher, W.A. Smith, M. Stefik, ACS Energy Lett. 3 (2018) 112–124.
[16] T.L. Kim, M.J. Choi, H.W. Jang, MRS Commun. (2018) 1–14.
[17] Q. Shi, S. Murcia-López, P. Tang, et al., ACS Catal. 8 (2018) 3331–3342.
[18] A.B. Murphy, P.R.F. Barnes, L.K. Randeniya, et al., Int. J. Hydrogen Energy 31 (2006) 1999–2017.
[19] Z. Li, W. Luo, M. Zhang, J. Feng, Z. Zou, Energy Environ. Sci. 6 (2013) 347–370.
[20] M. Zhou, H.B. Wu, J. Bao, et al., Angew. Chem. Int. Ed. 52 (2013) 8579–8583.
[21] J.H. Kim, J.S. Lee, Adv. Mater. 31 (2019) e1806938.
[22] Y. Li, X. Hu, J. Huang, et al., Acta Phys. Chim. Sin. 37 (2021) 2009022.
[23] Y. Liu, Y. Guo, L.T. Schelhas, M. Li, J.W. Ager, J. Phys. Chem. C 120 (2016) 23449–23457.
[24] C.C. Hou, T.T. Li, Y. Chen, W.F. Fu, ChemPlusChem 80 (2015) 1465–1471.
[25] R. Shen, D. Ren, Y. Ding, et al., Sci. China Mater. 63 (2020) 2153–2188.
[26] H. Zhang, B. Chen, H. Jiang, et al., Nanoscale 10 (2018) 12991–12996.
[27] D. Wu, Y. Wei, X. Ren, et al., Adv. Mater. 30 (2018) 1705366.
[28] Y. Pan, K. Sun, S. Liu, et al., J. Am. Chem. Soc. 140 (2018) 2610–2618.
[29] X. Yu, M. Wang, X. Gong, et al., Adv. Energy Mater. 8 (2018) 1802445.
[30] M.W. Kanan, D.G. Nocera, Science 321 (2008) 1072–1075.
[31] J. Liu, J. Li, M. Shao, M. Wei, J. Mater. Chem. A 7 (2019) 6327–6336.
[32] Z. Chen, Y. Ha, H. Jia, et al., Adv. Energy Mater. 9 (2019) 1803918.
[33] D. Zhao, H. Liu, X. Wu, Nano Energy 57 (2019) 363–370.
[34] S. Sun, Y. Sun, Y. Zhou, et al., Angew. Chem. Int. Ed. 58 (2019) 6042–6047.
[35] G.S. Hutchings, Y. Zhang, J. Li, et al., J. Am. Chem. Soc. 137 (2015) 4223–4229.
[36] T.W. Kim, M.A. Woo, M. Regis, K.S. Choi, J. Phys. Chem. Lett. 5 (2014) 2370–2374.
[37] J.R. Ding, K.S. Kim, Chem. Eng. J. 334 (2018) 1650–1656.
[38] L. Xia, J. Bai, J. Li, et al., Appl. Catal. B: Environ. 204 (2017) 127–133.
[39] N.A. Mohamed, H. Ullah, J. Safaei, et al., J. Phys. Chem. C 123 (2019) 9013–9026.
[40] S. Bai, H. Chu, X. Xiang, et al., Chem. Eng. J. 350 (2018) 148–156.
[41] Z. Ma, H. Hou, K. Song, et al., ChemElectroChem 5 (2018) 3660–3667.
[42] Z.Q. Liu, H. Cheng, N. Li, T.Y. Ma, Y.Z. Su, Adv. Mater. 28 (2016) 3777–3784.
[43] Y. Tang, R. Wang, Y. Yang, D. Yan, X. Xiang, ACS Appl. Mater. Interfaces 8 (2016) 19446–19455.
[44] J. Huang, Y. Zhang, Y. Ding, ACS Catal. 7 (2017) 1841–1845.
[45] J. Huang, G. Hu, Y. Ding, M. Pang, B. Ma, J. Catal. 340 (2016) 261–269.
[46] B. Klahr, S. Gimenez, F. Fabregat-Santiago, J. Bisquert, T.W. Hamann, J. Am. Chem. Soc. 134 (2012) 16693–16700.
[47] H. Huang, X. Li, J. Wang, et al., ACS Catal. 5 (2015) 4094–4103.
[48] Y. Lansari, J. Ren, B. Sneed, et al., Appl. Phys. Lett. 61 (1992) 2554.
[49] S.J. Wang, W.J. Lu, G. Cheng, et al., Appl. Phys. Lett. 94 (2009) 263106.